buildings

MDPI

Article

Damage Characteristics of Blasting Surrounding Rock in Mountain Tunnel in Fault Fracture Zones Based on the Johnson–Holmquist-2 Model

Lizhi Cheng [1], Zhiquan Yang [1,*], Ping Zhao [2] and Fengting Li [3]

[1] Faculty of Public Safety and Emergency Management, Kunming University of Science and Technology, Kunming 650093, China
[2] Shandong Province Transportation Planning and Design Institute Group Co., Jinan 250031, China
[3] School of Civil Engineering, Shandong University, Jinan 250061, China
* Correspondence: yzq1983816@kust.edu.cn

Abstract: Blasting is a widely employed technique for tunnel construction in mountainous regions; however, it often causes damage to the surrounding rock mass, particularly in fault fracture zones, which can lead to hazards such as rockfalls and collapses. This study examines the characteristics of damage to surrounding rock due to tunnel blasting through fault fracture zones. Based on an actual tunnel blasting construction project, we conducted a finite element analysis using the JH-2 material model, taking into account the width of the fault fracture zone. Results indicate that as the width of the fault fracture zone increases, the disturbance effect of tunnel blasting on the surrounding rock becomes more pronounced. Compared to the arch bottom and arch waist of the tunnel, the tunnel vault primarily absorbs the slip deformation and compressive forces resulting from blasting disturbances in the fault fracture zone. The findings of this paper contribute a valuable methodology for analyzing the mechanical mechanisms in mountain tunnel blasting and provide essential theoretical parameters to inform the design and construction of tunnel blasting projects.

Keywords: mountain tunnels; blasting construction; JH-2 model; numerical calculations

Citation: Cheng, L.; Yang, Z.; Zhao, P.; Li, F. Damage Characteristics of Blasting Surrounding Rock in Mountain Tunnel in Fault Fracture Zones Based on the Johnson–Holmquist-2 Model. *Buildings* **2024**, *14*, 3682. https://doi.org/10.3390/buildings14113682

Academic Editors: Guozhu Zhang and Bingxiang Yuan

Received: 13 October 2024
Revised: 7 November 2024
Accepted: 12 November 2024
Published: 19 November 2024

1. Introduction

During blasting construction of mountain tunnels through fault fracture zones, differential stress–strain variations are often induced in the surrounding rock, potentially leading to damage and failure of the tunnel structure. Understanding the dynamic deformation characteristics of the surrounding rock at fault fracture zones is crucial for ensuring safe construction through these complex areas. Currently, numerical methods are predominantly employed to study the mechanical behavior in mountain tunnel construction; however, the selection of an appropriate constitutive model tailored to tunnels crossing fault fracture zones remains uncommon.

Based on typical engineering practices, the vibration characteristics of tunnel secondary lining structures under the influence of fault zones were studied through the establishment of a finite element numerical model, and a vibration velocity safety criterion with stress as the control standard was proposed [1]. Using this stress criterion and an elastic–plastic ontological model, a statistical damage model of the rock mass was developed, allowing the study of cumulative damage evolution and distribution in grouted and reinforced peripheral rock under blasting and excavation conditions [2]. Applying fracture mechanics theory, a numerical simulation analysis investigated the dynamic response and vibration attenuation of surrounding rock during blasting and excavation near fault control zones, highlighting the impact of dynamic excavation on fault stability [3]. Geological and numerical analyses showed that the laminar-structured fault fragmentation zone presents a heterogeneous state, affecting stress redistribution in tunnels and contributing to significant

tunnel deformation [4]. Numerical simulations were conducted to assess surface blasting, analyzing changes in effective stress around and perpendicular to the blast hole under blasting loads [5]. Single and multiple full-face blasts were modeled by embedding a rock damage model into LS-DYNA R14.0 software through user-defined subroutines, with simulations verified against field test data [6]. The impact of millisecond delay blasting on surrounding rock damage was evaluated using acoustic testing and numerical simulation, with different detonator hole positions examined for their effects on surrounding rock integrity [7]. Cyclic blasting loads were analyzed for their effects on tunnel surrounding rock damage using a self-constructed physical model test system simulating high in situ stress conditions [8]. Additionally, the effects of millisecond delay blasting were investigated through a case study of the Chongqing North Avenue Tunnel [9]. Four scaled tunnel arch structures were fabricated and tested for anti-blast performance under internal explosions, with static load tests conducted on both undamaged and blast-damaged specimens to assess residual bearing capacities [10]. Finally, challenges in achieving smooth blasting results were addressed during the construction of the Liuzhi–Anlong Expressway Tunnel [11].

In summary, numerical calculation and analytical methods are predominantly applied to study the construction mechanics of tunnels traversing fault fracture zones. However, challenges remain regarding the selection of appropriate constitutive models and simulation techniques for blasting in these faulted areas. This research focuses on the blasting operations at the Lianfeng Tunnel entrance along the Dayong Expressway in Yunnan Province, China. Utilizing a finite element analysis program, JWL blasting theory, and the JH-2 material model, this study examines the characteristics of blast-induced damage to the surrounding rock. The findings aim to elucidate the deformation mechanisms in the surrounding rock due to tunnel blasting in fault fracture zones, offering valuable theoretical parameters and guidance for the design and execution of mountain tunnel blasting projects.

2. Numerical Calculation Models and Analysis Methods

To elucidate the dynamic deformation characteristics of blasting in the surrounding rock of a tunnel passing through a fault fracture zone, this study was conducted using the Lianfeng Tunnel Project on the Dayong Expressway in Yunnan Province, China as a case study.

2.1. Project Overview

The Lianfeng Tunnel on the Dayong Expressway is a separated double-bore tunnel with a vertical clearance of 5 m and a width clearance of 10.25 m. The tunnel alignment follows a nearly straight path with an axial direction of approximately 309°. The left bore, classified as a long tunnel, spans 10,984 m with a gradient of −2.600% and reaches a maximum depth of approximately 732 m at chainage K33 + 240. The right bore is similar in length at 10,995 m, also with a gradient of −2.600%, and reaches a maximum depth of about 748 m at chainage K33 + 190, beginning at K20 + 583 and ending at K31 + 578. The tunnel crosses the Lianfeng Fracture Zone (F12), which is the primary fracture structure in the survey area. This zone is characterized by northeast-trending faults oriented at approximately 40° to 45°, dipping between 310° and 315°, with fault surface inclinations of about 80° to 85°. The fracture exhibits clockwise torsional characteristics, affecting the strata from the Upper Aurignacian Unified Lamp Shadow Formation to the Lower Triassic Unified Feixiankuan Formation, with more significant damage to the latter. The faults encountered by the tunnel are highly destructive to the strata, impacting the surrounding rock, which is a moderately weathered gray rock with extensively developed joints. This rock mass is highly fractured with a brecciated structure and possesses extremely poor self-stabilizing capabilities. This is shown in Figure 1.

Tunnel construction employs conventional mine blasting techniques. In fault-fractured zones, the three-step construction method is utilized, with light surface blasting technology applied to strictly control over-excavation and under-excavation. The blasting advance should be determined based on the surrounding rock conditions, with excavation in

weak rock masses limited to 1–2 m per blast. During tunnel blasting, the step lengths should be adjusted according to the rock conditions: When the surrounding rock at the tunnel crown is unstable, construction support must closely follow the excavation. In such cases, extending step lengths can help reduce construction interference, ensuring quality excavation, effective support, and overall construction safety. The step height is set according to geological conditions, tunnel section dimensions, and other factors, with the initial height of the upper step set at 4.5 m, adjustable as needed during excavation. When constructing the steel frame for the upper step, measures such as widening the arch foot or using foot-locking anchors should be implemented to control surrounding rock deformation and secure the initial support. Excavation of the middle and lower steps should proceed only when the sprayed concrete on the upper step reaches at least 70% of its design strength. In cases of unstable rock, the pace should be shortened, and, if necessary, the middle and lower steps can be excavated in a staggered manner, with immediate application of initial support and arch. A composite lining structure is applied in the tunnel, with initial support including measures such as Φ8 mm steel mesh, a steel frame, C25 shotcrete, Φ22 mortar anchors, and Φ25 hollow anchors.

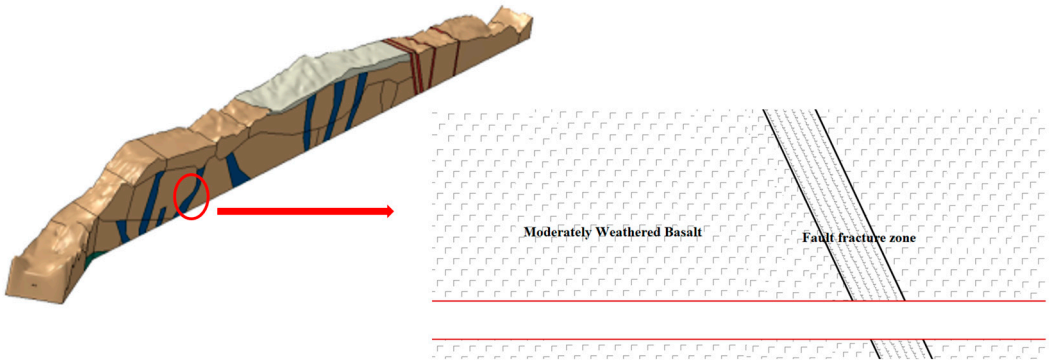

Figure 1. Schematic diagram of the distribution of fault fracture zones of Lianfeng Tunnel.

2.2. Rupture Modeling Theory

For explosion simulations, various equations of state have been developed to characterize the behavior of explosive products, with the Jones–Wilkins–Lee (JWL) equation of state widely recognized as one of the most comprehensive [12,13]. The JWL equation is frequently chosen in blasting analysis due to its effectiveness in modeling the dynamic response of high explosives, particularly in capturing pressure and volume changes during detonation. Tailored to simulate the rapid, high-pressure conditions of explosive detonation, JWL theory is instrumental in predicting the shockwave behavior immediately after detonation—essential for assessing blast impacts on surrounding structures. The parameters within the JWL equation are typically derived from empirical data specific to each explosive, allowing it to deliver validated, reliable results across a range of commonly used explosives. As it provides a more precise pressure–volume relationship for explosive gases than other general equations of state, the JWL equation is especially valuable for predicting damage and deformation in nearby structures, such as in tunnel construction.

The JWL equation, introduced in the 1960s by scientists John Paul Wierzbicki and John Wilkins, is particularly effective in modeling the strain energy changes in materials under compressive loads. It accurately characterizes the dynamic behavior of materials subjected to high pressures, elevated temperatures, and high strain rates, making it especially suitable for analyzing responses to dynamic loading scenarios, such as high-speed impacts and explosions. Due to its robustness, the JWL equation has become widely used in numerical simulations. The equation of state is expressed as follows:

$$P = Ae^{-R_1 V} + Be^{-R_2 V} + CV^{-(1+\omega)} \quad (1)$$

In the JWL equation, A, B, C, R_1, R_2, and ω are explosion constants, while v represents the relative volume v_1/v. These constants are typically determined by calibrating hydrodynamic simulation results against data from a cylindrical metal expansion test, commonly known as the Cylinder Test.

During the initial phase, the explosion products are extremely hot, especially as the gas undergoes adiabatic expansion, passing through the Chapman–Jouguet (CJ) point and entering the rapid expansion phase. At this stage, the behavior of the explosion products closely approximates that of an ideal gas. The energy contained in the explosion products during expansion can be expressed as follows:

$$e = \frac{A}{R_1}e^{-R_1V} + \frac{B}{R_2}e^{-R_2V} + \frac{C/\omega}{V^{\omega}} \tag{2}$$

The two formulas above share the same parameters, and the JWL equation of state, incorporating the energy term, can be derived through a system of simultaneous equations:

$$P = A\left(1 - \frac{\omega}{VR_1}\right)e^{-R_1V} + B\left(1 - \frac{\omega}{VR_2}\right)e^{-R_2V} + \frac{\omega e}{V^{\omega}} \tag{3}$$

The parameters in this equation, as well as the pressure and energy generated per unit volume of the explosion product in the CJ state and the detonation velocity, can be entered as input parameters in ABAQUS 2021.

2.3. Tunnel Blasting Constitutive Model

The choice of an appropriate material model is critical for the accuracy of numerical simulations. In geotechnical engineering, applying a model that closely replicates the stress–strain characteristics of actual structures is essential. Under blast loads, the surrounding rock in a tunnel typically transitions through elastic, plastic, and yielding phases before ultimately failing. Consequently, selecting a suitable constitutive model for rock damage is crucial. This study adopts the widely used Johnson–Holmquist-2 (JH-2) material model, developed by Gordon R. Johnson and Tim J. Holmquist, which introduces the Hugoniot Elastic Limit (HEL) to effectively characterize rock damage under blast impacts. The JH-2 model comprises three main components: a strength model, a damage model, and a set of corresponding polynomial equations.

Figure 2 presents the strength model of the JH-2 material constitutive model. Based on the damage factor D, the material is classified into three states: intact, damaged, and fractured. The standardized equivalent stresses corresponding to these states are depicted in the figure, with A, B, C, M, and N representing material parameters. Furthermore, T and p indicate the material's tensile and compressive strength limits, respectively.

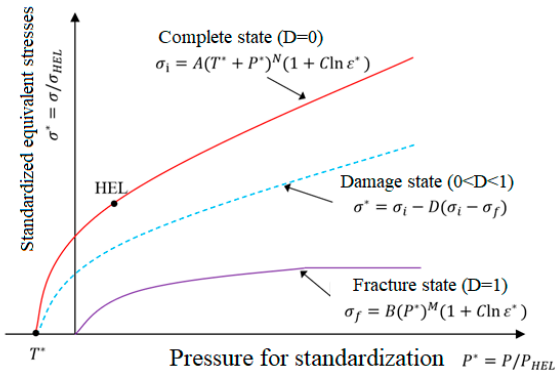

Figure 2. JH-2 material intrinsic model's strength model.

2.4. Selection of Mechanical Parameters

In this numerical simulation, the parameters for the JWL explosives are presented in Table 1, while the calculation parameters for the surrounding rock are derived from the field investigation report, with values provided in Table 2.

Table 1. Parameters of the JWL equation of state for emulsion explosives.

Density/ρ (kg·m^{-3})	Explosive Velocity/D (m·s^{-1})	A/GPa	B/GPa	R_1	R_2	ω	E_0/GPa
1600	6930	557.60	5.35	6.10	1.07	0.35	4.19

Table 2. Perimeter rock parameters.

	Density/ρ (kg·m^{-3})	Elastic Modulus/MPa	Poisson's Ratio	Cohesion/kPa	Internal Friction Angle
Moderately weathered basalt	2942	4372	0.23	214	33
Fault fracture zone	2574	273	0.28	97	25

The Johnson–Holmquist-2 model is commonly used to simulate the behavior of brittle materials under high-velocity impacts and high pressures. Determining the mechanical parameters for the JH-2 model involves a series of experimental and computational methods. The numerical calculation methods and mechanical parameters of the thesis mainly refer to the literature [14–16]. The specific rock mass parameters for the JH-2 model are shown in Table 3.

Table 3. Parameters of JH-2 constitutive model of the basalt rock mass.

ρ (kg·m^{-3})	*G*/MPa	*A*	*B*	*C*	*M*	*N*	*T*/MPa	*HEL*/GPa
2574	98.6	1.14	0.35	0.0049	0.65	0.682	43	3.3
P_{HEL}/GPa	β	D_1	D_2	K_1/GPa	K_2/GPa	K_3/GPa	σ_{Fmax}	\
2.28	1.0	0.005	0.6	43	−259	1203	0.24	\

A tunnel blasting model utilizes the Jones–Wilkins–Lee (JWL) equation of state to simulate the explosive blast process. The JWL equation effectively models the pressure exerted on the surrounding rock due to the explosion, capturing the explosive response and detonation characteristics. The detonation time and response of the explosive are influenced by the geometry of the charge, specifically the distance between the material point and the detonation point, and the velocity of the blast wave. The pressure generated during the explosive blast is described by the following equation:

$$p = A\left(1 - \frac{\omega\rho}{R_1\rho_0}\right)exp\left(-R_1\frac{\rho_0}{\rho}\right) + B\left(1 - \frac{\omega\rho}{R_2\rho_0}\right)exp\left(-R_2\frac{\rho_0}{\rho}\right) + \omega\rho E_m \quad (4)$$

where p is the blast pressure generated by the explosion; A and B are material constants of the explosive; R_{ho} is the density of the blast product; R_{ho} subscript 0 is the user-defined initial density of the explosive; ω is the Gruneisen parameter; R_1 and R_2 are dimensionless parameters; and E_m represents the initial internal energy of the explosive.

In ABAQUS/Dynamic-Explicit, the blast wave is applied to the numerical model cell through the combustion fraction.

$$F_b = min\left[1, \frac{\left(t - t_d^{mp}\right)C_d}{B_S L_e}\right] \quad (5)$$

where B_s is a constant (typically 2.5) that controls the width of the blast wave, ${t_d}^{mp}$ represents the time taken for the blast wave to reach the material point, L_e denotes the characteristic length of the cell, and C_d is the velocity of the blast wave in the explosive material. The pressure generated by the explosive is dependent on ${t_d}^{mp}$. If $t < {t_d}^{mp}$, the pressure remains zero; otherwise, the pressure is computed as the product of the pressure and the fraction of material burned, as described by the JWL equation. The time for the explosive blast wave to propagate is calculated using the following equation:

$$t_d^{mp} = min\left[t_d^N + \frac{\sqrt{\left(x^{mp} - x_d^N\right)\cdot\left(x^{mp} - x_d^N\right)}}{C_d}\right] \tag{6}$$

2.5. Numerical Calculation Models

According to the geological conditions and the actual situation of the project, the numerical simulation uses finite difference software Abaqus 2021 and establishes a three-dimensional calculation model, which intercepts two adjacent high-risk fracture zones on the mountain (480 m wide × 850 m long × 450 m high), with the widths of the two fracture zones of 67 m and 48 m, respectively, and the spacing of the zones of 73 m, and the tilt angle of 6°. In order to improve the quality of the grid, the tunnel is simplified into a circular tunnel with a diameter of 7.2 m, in which the spacing between the two tunnels is 40 m, the thickness of the lining structure is 0.7 m, and the support structure is established in accordance with the reinforcement diagram of the tunnel to support the inner and outer two ring steel frames, and different spacing of the steel frames is set for simulation. The mesh of the model is of C3D8R type. This is shown in Figure 3.

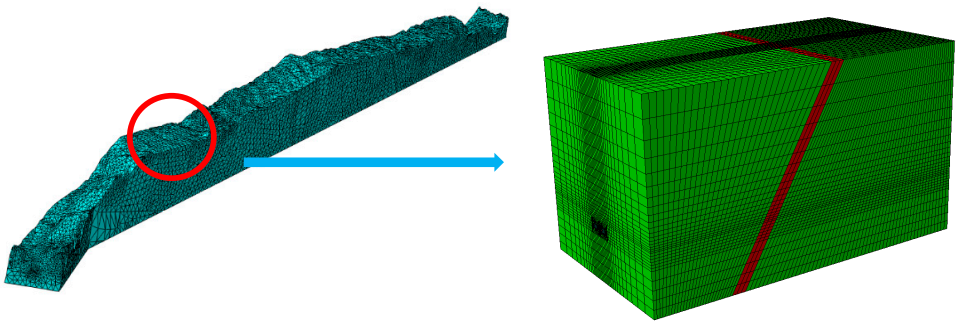

Figure 3. Numerical calculation model.

2.6. Numerical Calculation and Analysis Methods

To comprehensively simulate the damage patterns of two weathered granites under varying ground stresses during blasting, a series of detailed numerical simulations were conducted using ABAQUS finite element analysis software. This section outlines the critical steps of the numerical analysis process to ensure accurate and reliable simulation results. The key steps are as follows:

(1) Analysis Step Configuration: The numerical simulation comprises two analysis steps. In Step 1, the prestress field is imported to simulate ground stress under different peripheral pressures. Step 2 involves the blast simulation, where the duration of the analysis step is set to 4 ms, based on a review of experimental results and accuracy calculations [17].

(2) Boundary Conditions: To simulate the effect of geostress on rock blasting, static pressure is applied to the model. In addition to the pressure on the surface of the blast hole, vertical geostress is represented by static pressure in the Y direction, while horizontal geostress is represented by static pressure in the X and Z directions.

(3) Geostress Balancing: To accurately replicate the natural ground stress state, a static analysis is first performed. In this step, boundary conditions are applied to the same meshed rock model, and the resulting static stress is used to generate an ODB file. In the subsequent dynamic blast simulation, this file is used to create a prestress field. By

defining the loading steps and time points, the initial ground stresses for each rock unit are established before blasting.

(4) Contact Conditions: General contact between the components is defined using the Explicit method. Tangential and normal behaviors are specified, with friction behavior following the "penalty" formulation and a friction coefficient of 0.1. Normal contact behavior is defined as "hard contact".

(5) UMAT Subroutine: In the material module, the user material (UMAT) subroutine is invoked. The material model includes 32 attributes, and the non-independent variable function is called with eight solution-dependent state variables. The input file is generated, and material model parameters and output variables are defined by referencing the JH-2 model.

In tunnel blasting construction, analyzing the damage to surrounding rock with fault width as a variable is essential, as fault width directly affects the rock's capacity to absorb and distribute blasting energy. A wider fault zone typically contains weaker, more fractured rock, making it more susceptible to further damage, instability, and potential fracture propagation. In contrast, a narrower fault zone may better withstand blasting stresses but could also transmit shock waves more directly to adjacent areas, resulting in distinct damage patterns. Therefore, setting the fault zone's inclination angle as a fixed parameter and examining the surrounding rock damage and deformation characteristics by varying the fault width provide valuable guidance for actual project construction.

2.7. Reliability Analysis

Using the subway tunnel at Danshan Station in Qingdao as a case study, the JH-2 model was introduced as the constitutive model for the tunnel blasting simulation. The parameters of the JH-2 model specific to the local surrounding rock were obtained through experiments. Subsequently, numerical simulations and theoretical verifications were conducted to evaluate the safety distance of shotcrete based on various safety assessment criteria. The results demonstrate that this numerical calculation and analysis method can accurately assess the blasting damage characteristics of tunnel surrounding rock and serves as a valuable tool for engineering damage characterization [14].

3. Blasting Damage Characteristics of Tunnel Surrounding Rock in Fault Fracture Zones

3.1. Stress–Strain Characteristics of the Tunnel Surrounding Rock in Fault Fracture Zones

Figure 4 presents a cloud diagram illustrating the stress distribution in the surrounding rock caused by tunnel blasting across varying fault widths—specifically 10 m, 20 m, and 30 m. The figure highlights the following observations:

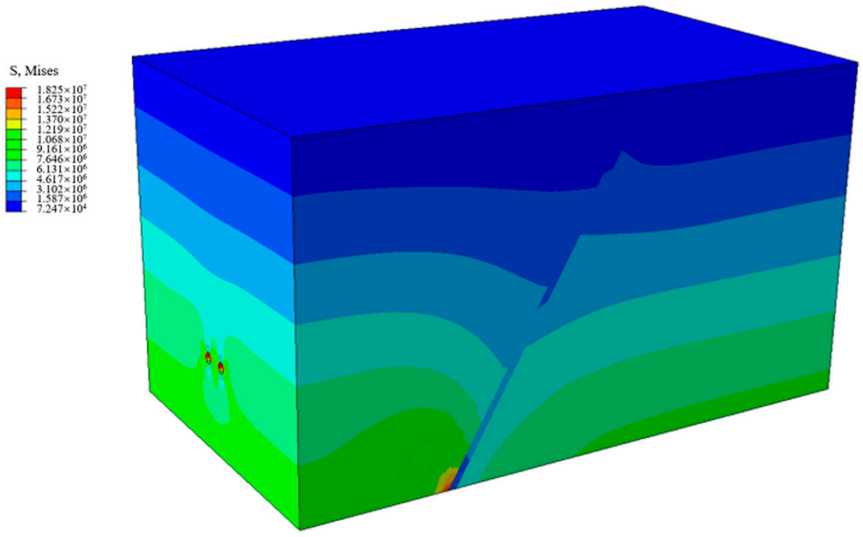

(**a**) Fault width of 10 m.

Figure 4. *Cont.*

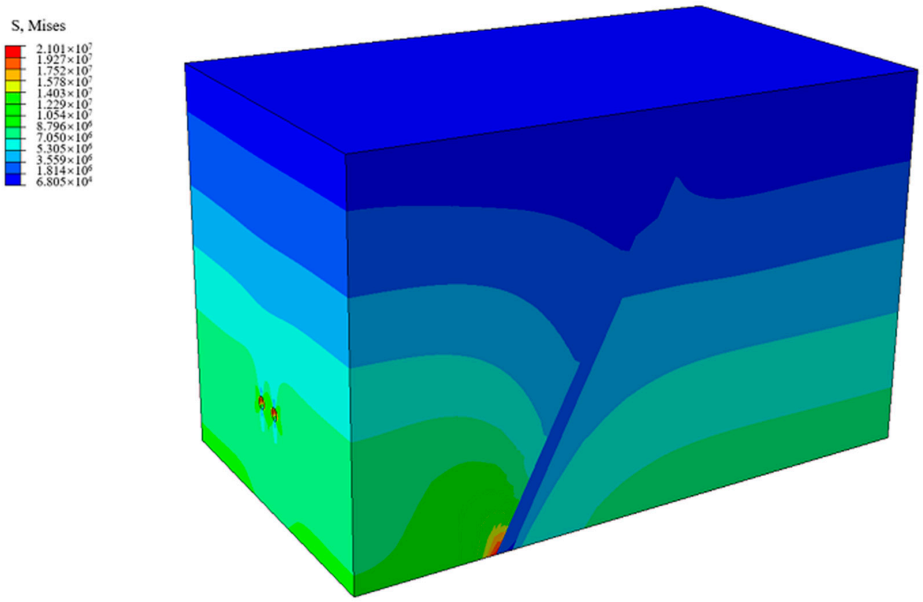

(**b**) Fault width of 20 m.

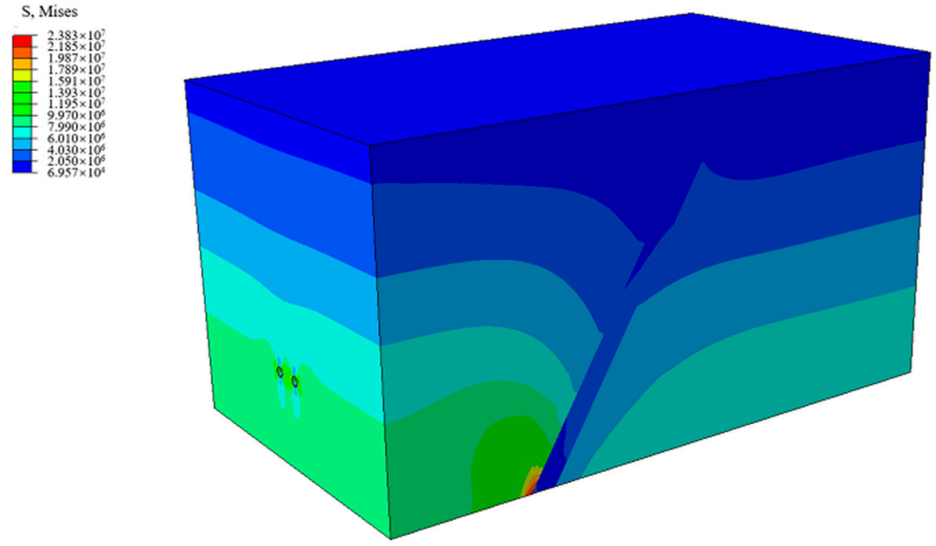

(**c**) Fault width of 30 m.

Figure 4. Stress distribution of surrounding rock induced by tunnel blasting in fracture area.

(1) Narrow Fault Widths: When the fault width is relatively small, the rock within the fault zone remains more intact, leading to stress concentration near the fault itself. This localized stress intensification can aggravate damage to the rock mass surrounding the tunnel, especially at the fault boundary where high-stress areas are likely to develop.

(2) Wide Fault Widths: In contrast, when the fault width is larger, the rock mass within the fault zone may already be highly fragmented or loosened. In such cases, the stress waves generated by blasting are absorbed or attenuated as they propagate through the fault. Consequently, stress variations within the fault zone are less significant, but the surrounding rock outside the fault can experience greater stress, particularly in the transition zone between the fault and the intact rock mass.

(3) Mechanical Properties of the Fault Zone: The mechanical characteristics of the rock within the fault zone (e.g., elasticity modulus and strength) often differ significantly from those of the surrounding intact rock. An increase in fault width results in notable

stress redistribution both inside and outside the fault zone. Wide faults tend to form large low-stress zones, while narrow faults contribute to high-stress concentration zones.

Given the concentration of stress in the surrounding rock, the tunnel support design must account for enhanced local reinforcement, particularly near the fault zone boundaries. This includes careful consideration of anchor placement, steel arches, and shotcrete application.

In conclusion, fault width plays a critical role in stress variation during tunnel blasting. Narrow faults typically lead to stress concentrations, while wide faults may induce slip within the fault zone and destabilize a broader area of the surrounding rock mass. Therefore, when tunneling through fault zones, it is essential to comprehensively evaluate fault width, surrounding rock mechanics, blasting methods, and support design to ensure the safety and stability of the construction.

Given the concentration of stress in the surrounding rock, the tunnel support design must account for enhanced local reinforcement, particularly near the fault zone boundaries. This includes careful consideration of anchor placement, steel arches, and shotcrete application. In conclusion, fault width plays a critical role in stress variation during tunnel blasting. Narrow faults typically lead to stress concentrations, while wide faults may induce slip within the fault zone and destabilize a broader area of the surrounding rock mass. Therefore, when tunneling through fault zones, it is essential to comprehensively evaluate fault width, surrounding rock mechanics, blasting methods, and support design to ensure the safety and stability of the construction.

Figure 5 presents a cloud diagram illustrating the longitudinal variation in surrounding rock strain caused by tunnel blasting across different fault widths (10 m, 20 m, and 30 m). The figure reveals several key observations:

(1) Strain Response in Narrow Faults: When the fault width is small, the fault absorbs and reflects less of the stress wave generated by blasting. As a result, stress is concentrated in the surrounding rock near the fault zone, leading to a more pronounced strain response, particularly in the transition areas on either side of the fault. This localized strain concentration can cause greater deformation in the surrounding rock post-blasting, especially at the tunnel vault and the sides of the excavation. In contrast, wider faults exhibit a different strain pattern. Due to the loose or fractured nature of the rock mass within the fault zone, the stress wave is attenuated and scattered, reducing stress transfer to the surrounding rock outside the fault. Consequently, the strain within the fault zone itself may be larger, while the surrounding rock outside the fault experiences a smaller strain response. This scenario typically results in a large plastic deformation zone within the fault, while the strain outside remains comparatively limited.

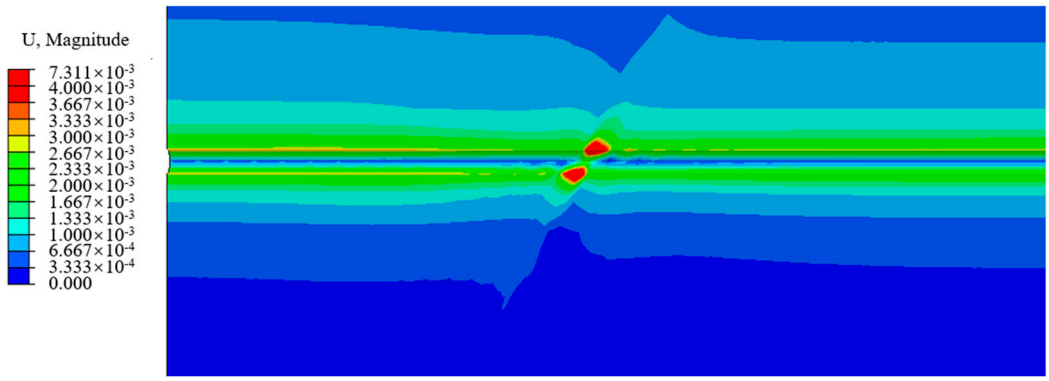

(**a**) Fault width of 10 m

Figure 5. *Cont.*

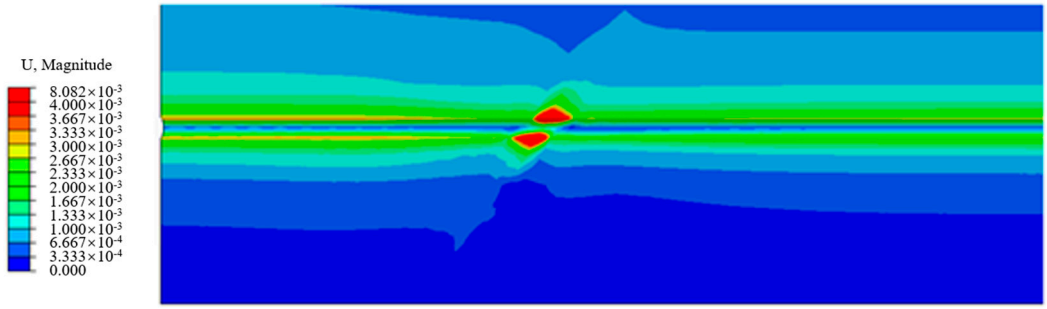

(**b**) Fault width of 20 m

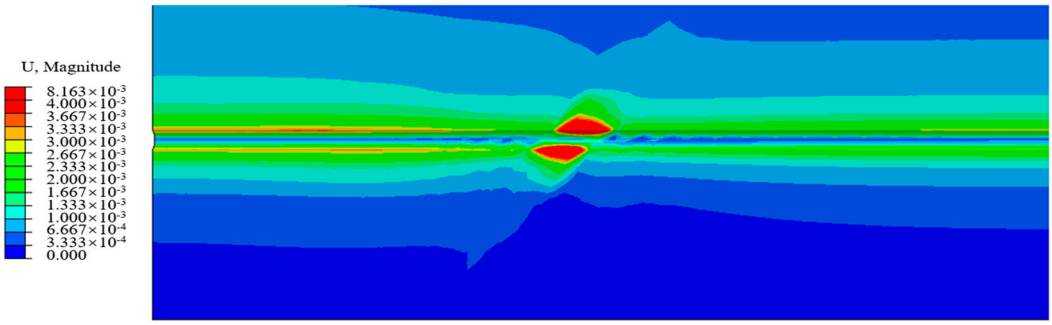

(**c**) Fault width of 20 m

Figure 5. Strain distribution of surrounding rock induced by tunnel blasting in fracture area.

(2) Deformation Characteristics of Narrow and Wide Faults: In narrow fault zones, where the rock is relatively intact, post-blast strain tends to concentrate locally around the fault, especially at the intersection of the tunnel and the fault. This strain concentration can lead to tensile or shear deformation, increasing the risk of localized damage to the surrounding rock. In contrast, within wide fault zones, the rock is generally looser or more fragmented, resulting in significant plastic deformation when the blast stress wave passes through. This leads to a wider strain distribution, characterized by an overall subsidence or extrusion deformation, rather than localized concentration.

(3) Asymmetry in Strain Distribution: When the tunnel intersects a fault, the width of the fault strongly influences the asymmetric distribution of strain in the surrounding rock. If one side of the tunnel is adjacent to the fault, strain concentration becomes more pronounced. In narrow faults, this strain asymmetry is more extreme, with greater differences in strain on either side of the tunnel. In contrast, wide faults tend to result in a more uniform strain distribution around the tunnel, although significant strain differences between the inside and outside of the fault zone persist.

(4) Support Design Considerations: The strain concentration caused by narrow faults may necessitate stronger tunnel support structures near the fault zone. High strain in localized areas may require additional anchors or shotcrete reinforcement to mitigate instability risks in the surrounding rock. Conversely, wide faults produce a broader strain distribution, meaning support design must account for the overall deformation characteristics of the fault zone. Reinforcement measures within wide fault zones, such as reinforced concrete structures or grouting, may be necessary to prevent large-scale plastic deformation and instability within the fault.

In conclusion, fault width has a significant impact on the strain distribution in surrounding rock during tunnel blasting. Narrow faults tend to concentrate strain and localize deformation, while wide faults result in a more extensive strain distribution and significant plastic deformation within the fault zone itself. Therefore, when tunneling through faults of varying widths, it is critical to accurately assess the surrounding rock strain, adjust blasting

parameters, and design appropriate support systems to ensure the safety and stability of tunnel construction.

3.2. Damage Characteristics of the Tunnel Surrounding Rock in Fault Fracture Zones

The propagation of stress waves is a highly complex process, characterized by reflection and refraction when the waves encounter interfaces between different media or structural boundaries. These interactions modify both the direction of wave propagation and the distribution of energy, potentially inducing tensile or shear damage in the materials involved. To assess the impact of stress wave propagation at the concrete–surrounding rock interface, a shear stress cloud diagram was generated (Figure 6), illustrating the X-Y cross-section located 1 m ahead of the tunnel face, 3 ms after blasting. The figure reveals several key observations: 3 ms after the blast, the stress wave reaches the concrete–surrounding rock interface, creating a significant stress differential between the two materials. The stress distribution along the concrete lining, resulting from surface blasting, is relatively uniform across the vault in the 0° to 180° range. However, the shear stress distribution is more complex, with internal shear stresses observed within the lining structure. The shear stress values range from −0.51 MPa to 0.50 MPa. When the opposing directional shear stresses exceed a critical threshold, slip deformation may occur at the cross-section. This slip can compromise the integrity of the concrete–surrounding rock interface, potentially reducing the stability of the concrete lining.

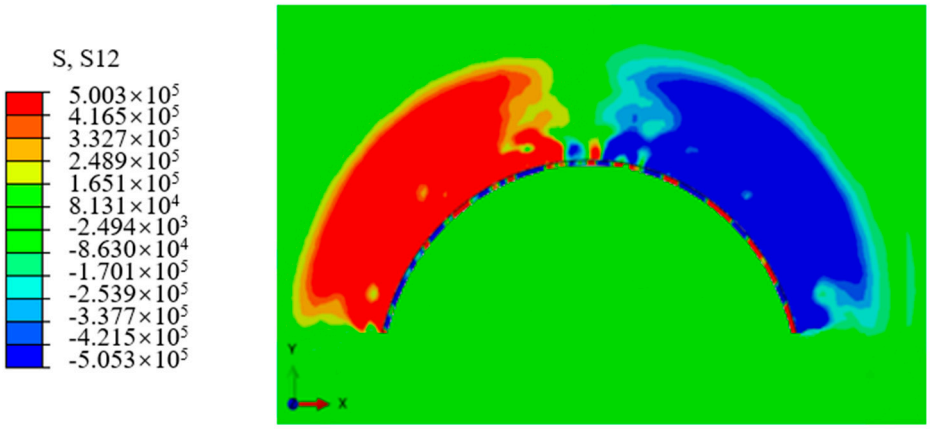

Figure 6. Shear stress cloud of X-Y section.

To assess the impact of stress differentials resulting from variations in body wave velocities across different media, a simulation was conducted. In this simulation, the JH-2 parameters for the surrounding rock material were adjusted to represent the characteristics of weathered granite, while the shear modulus of the lining structure remained unchanged. All other parameters were kept consistent. The resulting stress cloud diagram of the lining structure is shown in Figure 7. The figure indicates that the peak stress decreased from 15.86 MPa to 13.68 MPa, reflecting a reduction of 13.75%. The stress cloud diagram also shows that the C30 concrete support structure experiences rapid stress loading, with stress diffusion occurring at the stress wave interface. In contrast, the structure incorporating the modified rock material exhibits a more distinct stress wave interface, with minimal stress wave diffusion into the surrounding rock mass.

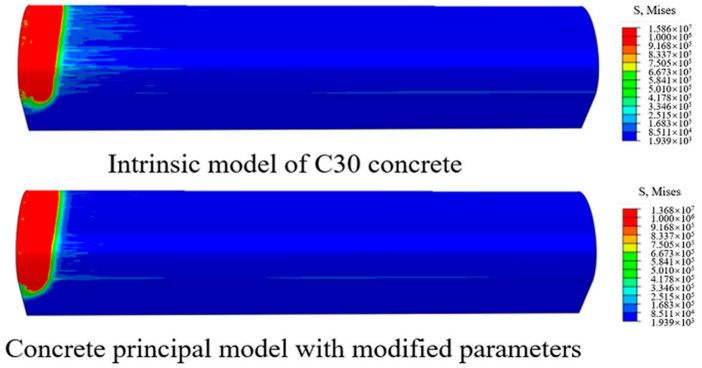

Figure 7. Stress diagram of lining structure.

3.3. Damage Characteristics of the Tunnel Lining Structures in Fault Fracture Zones

Figure 8 presents the circumferential strain curve of the tunnel lining under blasting conditions, with a fault width of 20 m and measured at distances of 1 m, 10 m, and 20 m from the tunnel face. In this diagram, positive strain values indicate deformation toward the interior of the tunnel, while negative values reflect deformation toward the exterior. The following observations are made from the figure:

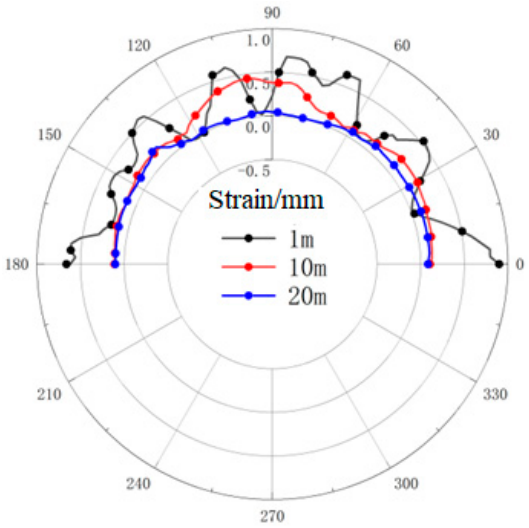

Figure 8. Circumferential strain curves of the tunnel blast lining structure with the distance of 1 m, 10 m, and 20 m from the palm face under the condition of 20 m fault width.

(1) 1 m from the Tunnel Face: At a distance of 1 m from the tunnel face, the lining arch experiences significant circumferential strain, primarily manifesting as compressive strain. This is due to the local stress concentration caused by the blasting-induced stress wave, which particularly affects the tunnel vault. The transient deformation of the surrounding rock results in compressive forces on the lining in the circumferential direction. If the lining design is insufficient to handle this strain concentration, cracks or localized failure may occur at the vault, compromising the structural integrity of the tunnel.

(2) 10 m from the Tunnel Face: At 10 m from the tunnel face, the circumferential strain is reduced compared to that at 1 m due to the attenuation of blast energy as it propagates through the rock mass. However, because of the large fault width and the highly fragmented nature of the surrounding rock, the tunnel lining is still subject to uneven pressure from the surrounding rock. This can result in localized strain concentrations at the arch of the tunnel, with the strain potentially shifting from compressive to tensile. This shift is especially pronounced when the blast stress wave interacts with the fragmented fault zone, which may weaken the overall stability of the lining structure.

(3) 20 m from the Tunnel Face: As the distance from the tunnel face increases to 20 m, the circumferential strain at the vault decreases further, and the deformation begins to stabilize. The long-term impact of the fault width on the lining structure manifests as gradual settlement and plastic deformation. Although the stress levels are lower at this distance and mainly present as uniformly distributed compressive strain or minor tensile strain, the presence of fractured rock within the fault zone still poses a significant risk of deformation, particularly near the fault edges.

In conclusion, the circumferential strain in the tunnel lining is highly influenced by the proximity to the tunnel face and the fault conditions. Close to the tunnel face, compressive strains dominate due to stress concentration, while further away, the strain reduces but becomes uneven due to the fault's fragmentation. The design of the tunnel lining must account for these variations to prevent structural damage, especially near the fault zone.

Characterizing tunnel arch damage is crucial, as the arch often experiences the highest stress concentration, particularly in fault zones or areas with disturbed surrounding rock. The arch serves as a primary load-bearing structure, supporting the overhead load from the surrounding rock. Damage to this component can compromise the tunnel's structural integrity, increasing the risk of progressive collapse or failure. During blasting, the arch is more susceptible to upward and lateral energy waves, which heighten the likelihood of fractures and spalling. In faulted zones, fractured rock may exert uneven pressure on the arch, intensifying stress points and aggravating damage. Such damage can significantly impact the tunnel's overall stability. By focusing on characterizing and mitigating arch damage, engineers can enhance the tunnel's capacity to sustain its designed loads and environmental conditions, ensuring both operational functionality and structural longevity.

Figure 9 illustrates the damage characteristics of the tunnel vault caused by blasting under fault zone conditions with a fault width of 20 m. Several key observations can be made from the figure:

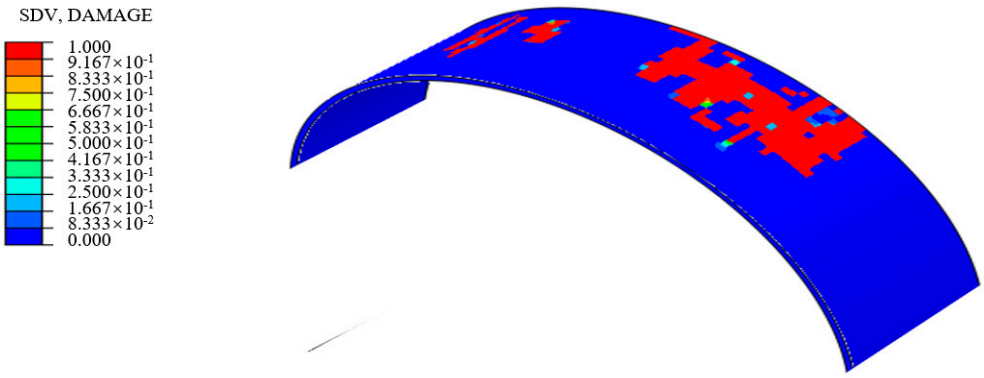

Figure 9. Characteristics of damage and destruction of the vault caused by tunnel blasting under the condition of fault width of 20 m.

(1) Stress Concentration Near the Tunnel Face: In the vicinity of the tunnel face, blasting generates a strong shock wave. This effect is particularly pronounced near fault zones, where the blasting energy leads to stress concentration. As the vault is a critical load-bearing element, it experiences significant circumferential stress, making it highly susceptible to stress concentration during the initial stages of blasting. This can lead to the initiation and propagation of micro-cracks and fractures in the early phases of tunnel excavation.

(2) Impact of Shock Wave Propagation in Fault Zones: As the shock wave travels through the fault zone, the fragmented nature of the rock disrupts the energy propagation path. This can subject the lining structure, particularly the vault, to increased dynamic loads. The high-frequency vibrations generated by the blast contribute to fatigue damage in the vault lining, causing microcracks to gradually expand. Over time, this can lead to crack propagation or material failure if left unaddressed.

In summary, with a fault width of 20 m, the primary damage mechanisms affecting the tunnel vault during blasting include local cracking due to stress concentration, spalling, and fragmentation induced by shock waves. To mitigate these risks, it is essential to enhance the tunnel lining design and implement reinforcement measures, such as anchoring and grouting, to address the complex geological conditions within the fault zone and the impact of blasting shock waves.

4. Conclusions and Recommendations

Tunnel construction in mountainous regions typically employs the blasting method. However, when tunneling through fault fracture zones, this method often results in significant damage to the surrounding rock. To address the geological hazards associated with tunnel blasting in faulted mountain areas, this thesis utilizes a large-scale finite element numerical simulation based on the JH-2 model. The study investigates the damage characteristics of the surrounding rock induced by blasting in fault-fragmented zones, with the Lianfeng Tunnel Project on the Dayong Expressway in Yunnan Province, China, serving as the case study. The findings provide a crucial theoretical foundation for the design and construction of mountain tunnels. The main conclusions of the study are as follows:

(1) Effect of Fault Width on Surrounding Rock Stress: The width of the fault has a significant influence on the stress changes in the surrounding rock during tunnel blasting. Narrow faults tend to cause stress concentrations, increasing the risk of localized rock bursts, while wide faults result in stress wave attenuation, potential fault zone slip, and instability over a broader area of the surrounding rock.

(2) Impact of Fault Width on Surrounding Rock Strain: The fault width also plays a critical role in determining the strain distribution in the surrounding rock. Narrow faults lead to localized strain concentrations and intense deformation, while wide faults cause a more extensive strain distribution, with significant plastic deformation occurring within the fault zone.

(3) Stress waves generated during blasting create stress differentials at the concrete–surrounding rock interface, leading to a complex shear stress distribution and potentially triggering slip-related damage. Utilizing lining materials with strength characteristics similar to those of the surrounding rock can effectively minimize damage at the cemented interface and enhance the overall structural stability of the tunnel.

(4) Vault Damage in Wide Fault Zones (20 m Width): When the fault width is 20 m, the primary damage characteristics of the tunnel vault include local cracking due to stress concentration, spalling, and fragmentation caused by the blasting shock wave, as well as settlement and localized collapse.

To mitigate damage and impact on the surrounding rock and supporting structures in tunnel blasting projects near fault fracture zones, specific countermeasures can be implemented. These strategies focus on enhancing stability, controlling destruction extent, and minimizing impacts on supporting structures. Key measures include controlled blasting techniques, pre-reinforcement of fault zones, enhanced monitoring and early warning systems, dynamic design adjustments, and strengthening of support structures. By integrating these countermeasures, tunnel projects can effectively manage and reduce blasting damage in fault fracture zones, thereby improving safety and extending the lifespan of supporting structures.

Author Contributions: Conceptualization, L.C.; Methodology, F.L.; Software, F.L.; Formal analysis, L.C.; Investigation, P.Z.; Resources, P.Z.; Data curation, F.L.; Writing—original draft, L.C.; Writing—review & editing, Z.Y.; Supervision, Z.Y. and P.Z. All authors have read and agreed to the published version of the manuscript.

Funding: This work was supported by Yunnan Asef-Han Academician Workstation Funded Programs (202105AF150076), Yunnan Provincial Key R&D Program Funded Projects (202003AC10002), and Yunnan Provincial Basic Research Program (202001AT070043).

Data Availability Statement: The original contributions presented in the study are included in the article, further inquiries can be directed to the corresponding author.

Conflicts of Interest: Author Ping Zhao was employed by the company Shandong Province Transportation Planning and Design Institute Group Co. The remaining authors declare that the research was conducted in the absence of any commercial or financial relationships that could be construed as a potential conflict of interest.

References

1. Xiao, K.; Zhou, C.; Zheng, X.; Xu, J. Blasting vibration characteristics and safety criteria of tunnel secondary lining under the influence of fault zone. *Eng. Blasting* **2021**, *27*, 130–139.
2. Lyu, G.; Zhou, C. Damage characteristics of grouted tunnel rock mass in fault zones induced by blasting. *Chin. J. Rock Mech. Eng.* **2021**, *40*, 2038–2047.
3. Wu, X.D.; Miao, X.M.; Gong, M.; Su, J.P.; Zhu, Y.Q.; Chen, X.L. Vibration safety threshold and control technology for blasting to prevent seawater intrusion in coastal tunnel sections near faults. *J. Mar. Sci. Eng.* **2024**, *12*, 1646. [CrossRef]
4. Sha, P.; Wu, F.Q.; Guo, Q.L. Anisotropic deformation in Muzhailing railway tunnel, Gansu, China. In Proceedings of the 3rd International-Society-for-Rock-Mechanics (ISRM) SINOROCK Symposium, Shanghai, China, 18–20 June 2013; pp. 855–860.
5. Yu, Y.Q.; Lu, Y.B.; Lu, Y.P. Numerical simulation of controlled perimeter blasting and field test on the fracture zones in Guanjiao tunnel. In Proceedings of the 2nd ISRM International Young Scholars' Symposium on Rock Mechanics, Beijing, China, 14–16 October 2012; pp. 57–63.
6. Ji, L.; Zhou, C.B.; Lu, S.W.; Jiang, N.; Gutierrez, M. Numerical Studies on the Cumulative Damage Effects and Safety Criterion of a Large Cross-section Tunnel Induced by Single and Multiple Full-Scale Blasting. *Rock Mech. Rock Eng.* **2021**, *54*, 6393–6411. [CrossRef]
7. Wang, M.; Liu, D.; Lu, X.; Hou, X. Blasting Damage of Large Section Tunnel to Surrounding Rock in Near Area. *Trans. Beijing Inst. Technol.* **2024**, *44*, 597–605.
8. Huang, J.; Chen, S.H.; Liu, M.L.; Li, K.P. Physical model test and numerical simulation study of cumulative damage to deep tunnel surrounding rock under cyclic blasting load. *Int. J. Damage Mech.* **2022**, *32*, 161–184. [CrossRef]
9. Liu, X.; Gong, M.; Yang, R.; Wu, X.; Wang, S.; Chen, X. Numerical analysis of surrounding rock damage caused by millisecond delay blasting of tunnel peripheral holes. *J. Vib. Shock* **2023**, *42*, 8–15.
10. Liu, Z.; Wu, J.; Cao, C.; Li, S.T.; Yan, Q.S. Dynamic performance and damage assessment of a shallow buried tunnel under internal explosion. *Tunn. Undergr. Space Technol.* **2023**, *133*, 104918. [CrossRef]
11. Qin, G.; Zeng, C.; Xu, J.; He, R. Numerical Simulation and Engineering Verification of Smooth Blasting in Limestone Tunnel Based on HJC Damage Constitutive Model. *Explos. Mater.* **2023**, *5*, 45–51.
12. Kury, J.W.; Hornig, H.C.; Lee, E.L.; McDonnel, J.L.; Ornellas, D.L.; Finger, M.; Strange, F.M.; Wilkins, M.L. Metal Acceleration by Chemical Explosives. In Proceedings of the 4th Symposium (International) on Detonation, White Oak, MD, USA, 12–15 October 1965; pp. 12–15.
13. Lee, E.; Finger, M.; Collins, W. *JWL Equation of State Coefficients for High Explosives*; Lawrence Livermore National Lab. (LLNL): Livermore, CA, USA, 1973.
14. Li, F.T.; Wu, K.; Li, S.R.; Wang, C.; Liu, Y.J.; Dou, Z.Y. Study on the dynamic response characteristics of lining structures in large-section tunnel blasting using JH-2 model analysis. *Sci. Rep.* **2024**, *14*, 10506. [CrossRef] [PubMed]
15. Liu, J.J.; Li, Y.; Zhang, H.J. Study on Shale's Dynamic Damage Constitutive Model Based on Statistical Distribution. *Shock. Vib.* **2015**, *2015*, 286097. [CrossRef]
16. Yang, Z.; Zhao, Q.; Gan, J.; Zhang, J.; Chen, M.; Zhu, Y. Damage evolution characteristics of siliceous slate with varying initial water content during freeze-thaw cycles. *Sci. Total Environ.* **2024**, *950*, 175200. [CrossRef] [PubMed]
17. Li, X.; Liu, K.; Yang, J.; Song, R. Numerical study on blast-induced fragmentation in deep rock mass. *Int. J. Impact Eng.* **2022**, *170*, 104367. [CrossRef]